ACS APPLIED MATERIALS & INTERFACES

Research Article

www.acsami.org

Elliptical Polymer Brush Ring Array Mediated Protein Patterning and Cell Adhesion on Patterned Protein Surfaces

Wendong Liu,[†] Yunfeng Li,[†] Tieqiang Wang,[†] Daowei Li,[‡] Liping Fang,[†] Shoujun Zhu,[†] Huaizhong Shen,[†] Junhu Zhang,[†] Hongchen Sun,[‡] and Bai Yang*[,†]

[†]State Key Laboratory of Supramolecular Structure and Materials, College of Chemistry, Jilin University, Changchun 130012, People's Republic of China

[‡]School of Stomatology, Jilin University, Changchun 130041, People's Republic of China

Supporting Information

ABSTRACT: This paper presents a novel method to fabricate elliptical ring arrays of proteins. The protein arrays are prepared by covalently grafting proteins to the polymer brush ring arrays which are prepared by the techniques combining colloidal lithography dewetting and surface initiated atom-transfer radical polymerization (SI-ATRP). Through this method, the parameters of protein patterns, such as height, wall thickness, periods, and distances between two elliptical rings, can be finely regulated. In addition, the sample which contains the elliptical protein ring arrays can be prepared over a large area up to 1 cm^2, and the protein on the ring maintains its biological activity. The as-prepared ring and elliptical ring arrays (ERAs) of fibronectin can promote cell adhesion and may have an active effect on the formation of the actin cytoskeleton.

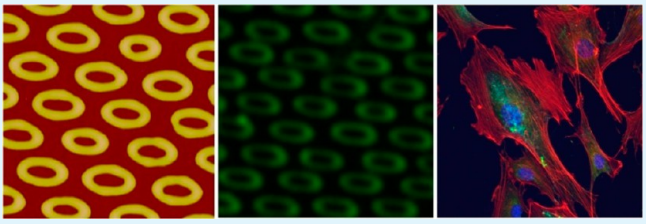

KEYWORDS: *polymer brush, protein patterns, elliptical ring arrays, cell adhesion*

1. INTRODUCTION

Fabrication of the patterned surfaces with distinct chemical contrast and finely controlled morphology is of great interest because it can be widely used in the fields of electronic,[1] magnetic,[2] chemical,[3] and biological sensors.[4−10] In particular, proteins and other biomolecules patterns which have a feature size of nanometer or sub-micrometer have been widely used in the fields of biosensors, drug screening, biomedical interfaces, tissue engineering,[11] artificial growth of neuronal networks,[12−14] and research of cell biology.[15−19] Furthermore, the ordered or disordered nanopatterns possess great advantages, such as higher amount of reaction sites and much smaller sample dosage compared with the microarrays. As a result, the nanopatterns lead an enhanced detection sensitivity with reduced quantities of analytes and reagents, as well as improved kinetics.[20] For instance, protein and DNA patterns in nanoscale can be used to characterize the proteome and genome content in a highly parallel manner, which has promoted the development of the medical diagnostic technologies.[21]

In the past decade, the patterned polymer brushes have got a great development. The polymer chains extend from the surface, making themselves sufficiently dense and leading to highly steric crowding, which results in an entropically unfavorable conformation. And several methods have been used to fabricate polymer brush patterns, which combined the controlled surface-initiated polymerization with lithography techniques, such as photolithography, electron-beam lithography, scanning probe microscopy lithography, soft lithography, and Langmuir−Blodgett lithography.[22−39] As a result, patterns with a feature size of 100 nm have been produced by nanoimprinting lithography[40−42] and modified microcontact printing.[43] However, they cannot be used to fabricate polymer brush patterns with large area at a low-cost and in a time efficient manner. Moreover, finely controlling the structure parameters, such as compositions, shapes, and dimensions of the features, is a key point for the polymer brush patterns to be applied in the fields of macromolecule sensors, novel micro- or nanofluidic devices, and biomacromolecule patterns for protein and cell studies. In addition, it is still a major challenge to develop a cost- and time-efficient method to fabricate protein patterns in high-throughput and activity manner, especially for those with both micrometer and nanometer features in one sample, and a background of stable protein-resistant.

During these years, micro- and nanoring arrays are proposed to be of great importance and have attracted great interest in many scientific and technological fields.[44−50] Due to the efficient-process methods to fabricate arrays, the structure parameters could be modulated via varying their diameter, wall thickness, and arrangement.[51,52] Few works are focused on exploiting the ring structures to fabricate polymer/biomolecules arrays. It is highly significant to develop an efficient method to

Received: September 10, 2013
Accepted: November 20, 2013
Published: November 20, 2013

prepare biomolecule arrays for biological studying. In this paper, we report a simple and cost-efficient method to fabricate protein patterns via covalently grafting protein to elliptical poly(2-hydroxyethyl methacrylate) (PHEMA) brush ring arrays over a large area of nearly 1 cm^2. The elliptical PHEMA brush ring arrays were fabricated by the method of combined colloidal lithography dewetting with surface initiated atom-transfer radical polymerization (SI-ATRP) as shown in Figure 1. By

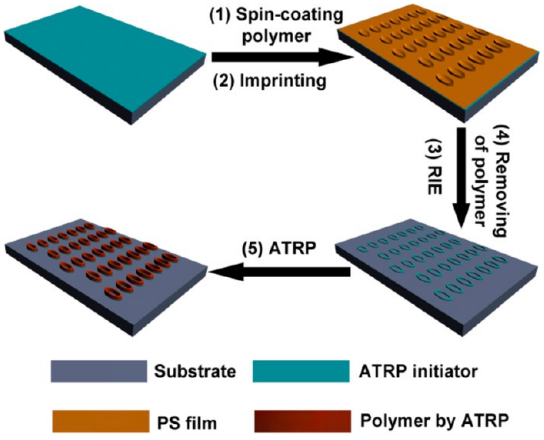

Figure 1. Typical procedure of preparing patterned ring polymer brush.

this method, the parameters such as wall thickness, distances between two PHEMA rings, and height of the elliptical ring arrays, with their respect ratio altered from 1 to 2.5, can be well controlled via regulating the process of colloidal lithography dewetting and the parameters of the polymerization process. Also, this method can be used to fabricate some inorganic, metal, or responsive material ring structures which can be applied in the fields of photonics, electronics, and magnetics. More importantly, the elliptical protein ring patterns are fabricated after protein covalently grafting to the polymer brush, and the proteins on the ring maintain their biological activity. This covalent grafting method can efficiently avoid the unfolding and partial denaturation of the protein patterns which were prepared by adsorption.[56,57]

2. EXPERIMENTAL SECTION

2.1. Materials. Silicon wafers (100) and fused silica wafers were cut in ca. 2.0 × 2.0 cm^2 pieces and soaked in a piranha solution (a mixed solution of concentrated H_2SO_4 and 30% H_2O_2 with the volumetric ratio 7:3) for 30 min under boiling (***Caution***: strong oxide) to make the surface hydrophilic, and then they were rinsed with deionized water for several times and at last dried with nitrogen gas (N_2) stream. 2-Hydroxyethyl methacrylate (HEMA) monomer, 2,2′-bipyridine, phosphate buffer saline, and copper(II) bromide ($CuBr_2$) were provided by Alfa Aesar. Polystyrene (PS, M_W = 280 000), 3-aminopropyltrimethoxysilane (APTMS), 2-bromoisobutyrylbromide, 4-dimethylaminopyridine (DMAP), *N*,*N*′-disuccinimidylcarbonate (DSC), copper(I) chloride (CuCl), tetramethylrhodamine B isothiocyanate (TRITC) labeled phallaoidin, 4,6-diamidina-2-phenylindole (DAPI), albumin from bovine serum, and anti-vinculin were purchased from Aldrich. PDMS elastomer kits (Sylard 184) were purchased from Dow Corning (Midland, MI). Poly(ethylene glycol)-silane (PEG-silane) (M_W = 1000) was provided by Shanghai Yare Biotech. Fibronectin (FN) was provided by the Shanghai EYSIN Biotechnology. Polyoxymethylene (4%), Triton-X100, human immunoglobulin G (IgG), FITC-labeled goat anti-human IgG, FITC-labeled BSA, and FITC-labeled rabbit anti-mouse IgG were purchased from Beijing DINGGUO Biotechnology. Dichloromethane, toluene, triethylamine, absolute ethanol, *N*,*N*-dimethylformamide (DMF) and the four components of the photoresist were used as received. The water used in all experiments was deionized and doubly distilled prior to use.

2.2. Fabrication of the Elliptical Initiator Ring Arrays. The $-NH_2$ groups were grafted onto the silicon and fused silica wafers by gas-phase growth method as demonstrated in our previous work.[53] In brief, the wafers were placed in a sealed vessel in which several drops of APTMS were dropped on the bottom, while the wafers and the drops were separated. Then the vessel was heated for 1 h at 60°C in an oven to make the $-NH_2$ grafted onto the wafers via the chemical reaction between APTMS vapor and the −OH groups on the silicon or fused silica wafers. Then the $-NH_2$ group modified wafers were immersed in the mixed solution of 10 mL anhydrous dichoromethane and 140 μL triethylamine, followed by adding 100 μL of 2-bromoisobutyryl bromide (the ATRP initiator) into the solution containing the $-NH_2$ modified wafers at 0 °C. The sealed vessel was left at this temperature for 1 h and then placed at room temperature for 15 h. The wafers were rinsed with anhydrous dichoromethane and absolute ethanol, and then dried by N_2 stream.

The initiator elliptical ring arrays were fabricated by colloidal lithography dewetting. First, the ATRP initiator grafted wafers covered by a layer of PS were prepared via spin coating the toluene solution of PS with the concentration of 6 $mg{\cdot}mL^{-1}$ onto the wafers. Then the elliptical PS ringlike arrays were prepared on the surface of the initiator covered wafer by colloidal lithography dewetting method. In brief, after spin-coating the PS film onto the substrate, a resin mold of EHAs (elliptical hemisphere arrays) was compressed onto the surface of the sample under a $1{\times}10^3$ Pa pressure to make the thickness of the PS film attached to the down side of the EHAs thinner, because it flows to the space between the arrays to form elliptical ringlike PS arrays. Finally, the elliptical initiator ring arrays were achieved via etching off the interconnecting flashing layer (the PS film inside and between the PS rings with a thinner thickness than the rings) of the elliptical PS ringlike arrays and the exposed initiators by the oxygen reactive ion etching (RIE), which was performed using Plasmalab 80 Plus instrument (Oxford Instrument). In this work, the RIE operating at 10 mTorr pressure, 50 SCCM oxygen gas flow rate, and RF power of 60 W, ICP power of 0 W was carried out from 60 to 90 s. After the RIE process, the retained PS were removed by DMF under ultrasonic bath.

2.3. Preparing Polymer Brush Patterns by the Method of Grafting from Surfaces. In this experiment, HEMA was chose as the monomer to prepare polymer brush patterns via the method of grafting from surfaces. For the polymerization of PHEMA, 36 mg (0.16 mmol) of $CuBr_2$ and 244 mg (1.56 mmol) of 2,2′-bipyridine were added to 8 mL of aqueous monomer solution (the volumetric ratio of HEMA/H_2O equals 1:1), and the mixtures were shaken in an ultrasonic bath until a homogeneous blue solution formed. The mixtures were degassed for 30 min by ultrapure N_2 flow, 55 mg (0.55 mmol) CuCl was added into the solution, and then it was shaken in an ultrasonic bath until the color of the solution changed into dark brown. Lastly, the wafers with initiators were immersed in the solution from 1 to 12 h under nitrogen flow at room temperature. After polymerization, the samples were cleaned by using absolute ethanol and DMF via washing several times.

2.4. Preparing the Patterns of Protein−Polymer Conjugates and Negative Control Experiments. Before the polymerization of PHEMA in this part, the wafers with elliptical ATRP initiator ring arrays were immersed in the toluene solution of PEG-silane (M_w = 1000) with the concentration of 0.05 $mg{\cdot}mL^{-1}$ for 12 h at room temperature for the purpose of reducing the protein nonspecific absorption on the background. The wafers were then rinsed with toluene and absolute ethanol for several times and dried by N_2 flow. Then PHEMA was grafted from the surface by the method of SI-ATRP. After that, the elliptical ring arrays of protein−polymer conjugates were prepared by the coupling reaction between PHEMA and protein which is mediated by DSC. In brief, The samples were immersed in the solution of 0.1 M DSC and DMAP in anhydrous

DMF and then were deoxygenated by ultrapure N_2 flow for 24 h. The samples were rinsed thoroughly with DMF and dichloromethane, and then dried by N_2 flow. For the conjugation of proteins to the polymer brush, the modified samples were immersed in a solution of human IgG (50 $\mu g \cdot mL^{-1}$) or fibronectin (FN) (50 $\mu g \cdot mL^{-1}$) in phosphate buffered saline (PBS, pH = 7.4) for 2 h at room temperature. After that, the wafers were rinsed with PBS several times to remove the physically absorbed proteins on the surfaces of the samples.

To confirm that the human IgG covalently grafted to the polymer brush, a negative experiment was performed as follows: the wafers with polymer brush ring arrays without succinimidyl modification were immersed in a solution of human IgG (50 $\mu g \cdot mL^{-1}$) for 2 h at room temperature. After that, the wafers were treated with ultrasonication for 30 s and rinsed with PBS several times to remove the physically absorbed proteins on the surfaces of the samples.

To evaluate the biological activity of the human IgG on the elliptical ring arrays, the wafers with elliptical human IgG ring arrays were immersed in a solution of FITC-labeled BSA (50 $\mu g \cdot mL^{-1}$), FITC-labeled rabbit anti-mouse IgG (50 $\mu g \cdot mL^{-1}$), and FITC-labeled goat anti-human IgG (50 $\mu g \cdot mL^{-1}$) in PBS for 1.5 h. And then the wafers were treated with ultrasonication for 30 s and rinsed using PBS for several times to remove the nonspecifically absorbed proteins.

2.5. Cell Seeding and Staining. Mouse MC3T3-E1 osteblasts were plated at a density of 3×10^4 cells/mL in H-DMEM media supplemented with 10% fetal bovine serum (FBS) (Gibco) and 1% antibiotics (25.000 IU·mL^{-1} penicillin and 25 mg·mL^{-1} streptomycin) in 5% CO_2 at 37 °C. After culturing for 12 h, cells on the substrates were washed in PBS to remove the physical absorbed organics and prepare for stain. For cell immunostaining, the cells were fixed with 4% polyoxymethylene in PBS solution for 20 min and then permeabilized with 0.1% Triton X-100 for 10 min. After that the cells were incubated in a 3% bovine serum albumin blocking agent for 2 h at room temperature and washed twice with PBS buffer. Mouse monoclonal anti-vinculin with a concentration of 1.25 $\mu g \cdot mL^{-1}$ was added to the cells and incubated at 4 °C for 12 h and then washed three times in PBS. FITC-conjugated goat anti-mouse IgG (10 $\mu g \cdot mL^{-1}$) and TRITC-phalloidin (37.5 ng·mL^{-1}) were added to the surfaces and incubated for 60 min at room temperature. Cells were thereafter washed three times with PBS, incubated with 2 $\mu g \cdot mL^{-1}$ DAPI for 5 min at room temperature, and then washed three times. Stained cells were kept in PBS at 4 °C.

2.6. Characterization. Atomic force microscopy (AFM) images were recorded in tapping mode with a Nanoscope IIIa scanning probe microscope from Digital Instruments under ambient conditions. The fluorescent images of elliptical protein ring arrays were taken by using an OLYMPUS BX51 instrument. The confocal fluorescent microscopy images of the cells cultured on the ring and elliptical ring patterns were taken by using the laser scanning confocal microscope OLYMPUS BX81 (FluoView FV1000).

3. RESULTS AND DISCUSSIONS

3.1. Fabrication of the Elliptical PHEMA Ring Arrays by Colloidal Lithography Dewetting and SI-ATRP. The elliptical PHEMA brush ring arrays are fabricated by grafting the PHEMA from the surfaces which were modified by elliptical ring ATRP initiator arrays. Figure 1 shows the schematic illustration of this process. Firstly, the mold which will be used for colloidal lithography dewetting was prepared (Figure S3, Supporting Information). In brief, we used the two-dimensional (2D) non-close-packed (ncp) colloidal monolayers of 1 μm silica spheres as original templates to fabricate poly(dimethysiloxane) (PDMS) well arrays. The PDMS molds were stretched to a certain direction to turn the spherical well arrays into elliptical ones after they were peeled off from the ncp templates for the purpose of fabricating photopolymerizable resin elliptical hemisphere arrays (EHAs) which will be used as the template to fabricate elliptical ring arrays. To fabricate the photopolymerizable resin EHAs, the stretched PDMS molds were coated with a thin film of oligomer via spin-coating. After the polymerization of the oligomer under UV exposure, the PDMS mold was peeled off and the photopolymerizable resin EHAs template achieved. Figure S4 shows the scanning electron microscopy (SEM) images of original 2D-ncp colloidal crystals used to fabricate the PDMS mold, AFM images of 2D hexagonal ncp nanowells on the PDMS mold, and SEM image of the photopolymerizable resin EHAs template used for micromolding. The images indicate that the photopolymerizable resin EHAs were successfully fabricated and the ordering property of the ncp template was maintained. Then the photopolymerizable resin EHAs template was compressed onto the initiator modified substrate coated with a 20 nm PS film under a pressure of about 1×10^3 Pa while the PS film was prepared by spin-coating a 6 mg·mL^{-1} toluene solution of PS onto the substrate. After that the EHAs template and the substrate were heated for 3 h at 100 °C in an oven while maintaining the pressure. During this process, the polymer performs a flow state when the temperature is above the glass-transition temperature (T_g) of the PS. Thus, with the help of the capillary force caused by the narrow spaces between EHAs and substrate, the flow state PS will flow into the narrow spaces and dewet around the surface of the EHAs template to form the ringlike morphology. After cooling down the system to room temperature and peeling off the EHAs template, the elliptical PS ring arrays were achieved including the PS flashing layers both inside and outside the ridge of the ring structure. Then after the redundant flashing layer of PS and the initiators exposed both inside and outside, the elliptical ring structures were removed via RIE treatment, the remaining PS ring arrays were washed off with toluene, and then the elliptical ATRP initiator ring arrays were achieved. Finally, the elliptical PHEMA ring arrays were prepared via grafting the PHEMA from the surface modified with elliptical initiator ring arrays by the method of SI-ATRP.

Figure 2 shows the AFM images of the elliptical PHEMA ring arrays fabricated by the above method. The 3D AFM

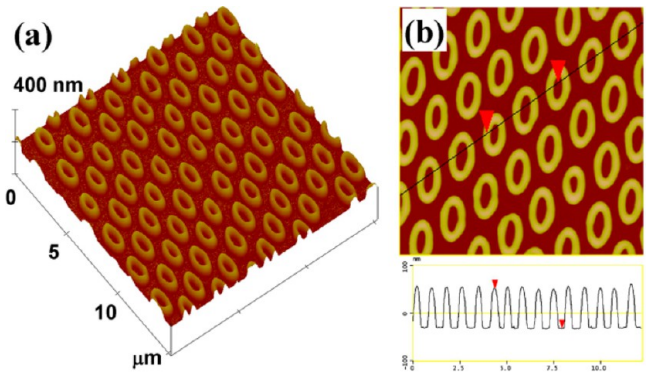

Figure 2. (a) 3D AFM images of patterned PHEMA brush elliptical rings. (b) AFM images of patterned PHEMA brush elliptical rings and cross-sectional analysis; z scale is 200 nm, and sizes are 10 μm × 10 μm.

image of the elliptical PHEMA brush ring arrays in Figure 2a shows that the elliptical polymer brush ring arrays exhibit hexagonal ncp and homogeneous architectures over large areas which can be larger than 100 μm^2. Also, using this method, the sample area which contained the ring arrays can reach 1 cm^2 though there are some defects. Figure S5 shows the AFM images that were collected from the 1 cm^2 sample from five

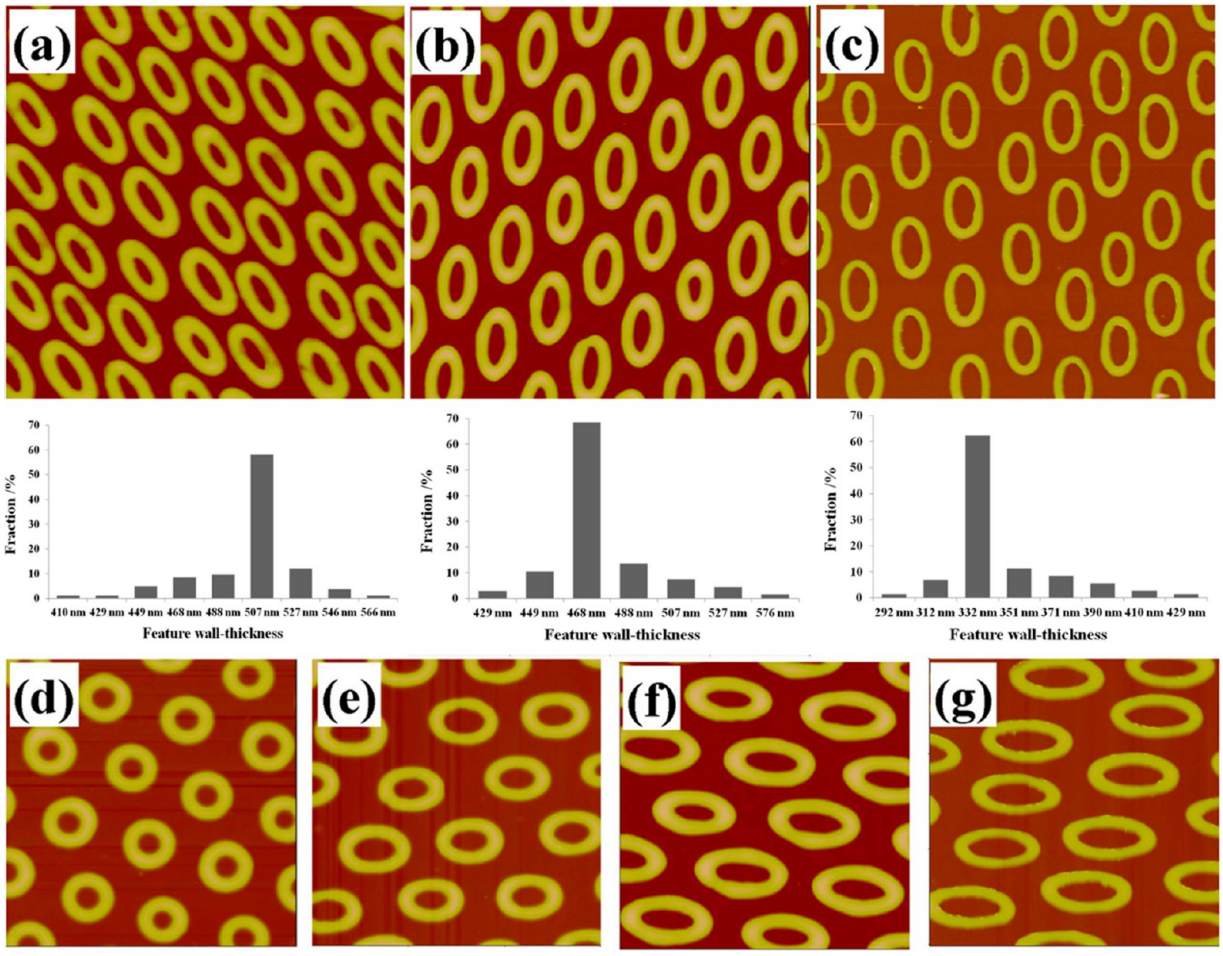

Figure 3. (a–c) AFM images of PHEMA brush patterns grafting from ATRP initiator patterns after 30, 60, and 75 s etching. Sizes are 10 μm × 10 μm; the statistical graph below each image shows the feature wall-thickness distribution of the elliptical rings. (d–g) AFM images of PHEMA brush patterns with different aspect ratios. Sizes are 6 μm × 6 μm.

locations that distributed at the center and four corners; these images indicate that the elliptical ring arrays maintain the ordering property which can reach 100 μm^2 over 1 cm^2 area. Moreover, the wall thickness of the ring is uniform and the polymer brush ring arrays are vertical to the substrates. The cross-sectional analysis of the elliptical PHEMA brush ring arrays in Figure 2b demonstrates that the height of the ring is about 84 nm with the aspect ratio about 2. These prove that the elliptical PHEMA brush ring arrays have been successfully fabricated over a large area. This method provides a new way to fabricate complex polymer brush structures. In addition, with the help of SI-ATRP, ring arrays consisting of different kinds of polymers can be successfully prepared and the application of functional polymer patterns will be widened.

3.2. Fabrication of the Elliptical Polymer Ring Arrays with Tunable Height and Aspect Ratio. As we know that the attractive properties of elliptical ring arrays are greatly depended on the geometric parameters of the ring, thus it is meaningful to fabricate elliptical ring arrays with different physical features via modulating the geometric parameters during the fabrication process.

In this experiment, the feature structure of the polymer ring arrays can be finely controlled by regulating the experimental conditions. For the samples having the same aspect ratio, the feature structure of the elliptical ring arrays can be precisely modulated by regulating the etching time of the RIE process. Figure 3a–c shows the AFM images of the elliptical polymer brush ring arrays with the same aspect ratio and different wall thickness of the ring structure. The different wall thickness is caused by the different etching time during the process of fabricating the elliptical ATRP initiator ring arrays via removing the flashing layer of PS and the exposed ATRP initiators by the RIE treatment. The etching time was 30 s (Figure 3a), 60 s (Figure 3b), and 75 s (Figure 3c). From the AFM images, we can get the information that the wall thickness of the polymer brush ring decreased as the etching time increases during the process of initiator etching. The wall thickness of the elliptical rings in each image were measured, and the results show that the major wall thicknesses are 507 nm (Figure 3a), 468 nm (Figure 3b), and 332 nm (Figure 3c). These results indicate that the wall thickness of the ring structure can be continuously regulated via choosing the appropriate conditions and etching time in the RIE step.

Moreover, due to the excellent elastic property of the PDMS which guarantees the freedom of structure changing, we can achieve elliptical well arrays with different aspect ratios which can be adjusted in a certain range via changing the force applied to stretch the PDMS well arrays during the process of EHAs fabrication. Figure 3d–g shows the AFM images of the elliptical PHEMA brush ring arrays with different aspect ratios which were fabricated by PDMS micromolds which were stretched under different forces. As shown in the images, when no force

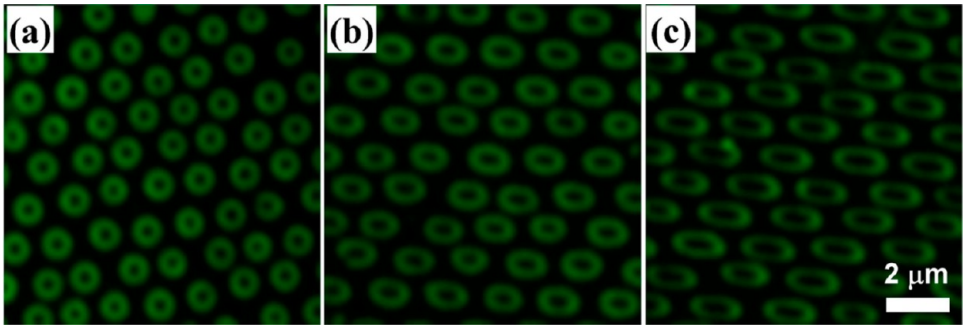

Figure 4. Fluorescent photographs of the IgG ring patterns with aspect ratios 1 (a), 1.5 (b), and 2.5 (c) after bonding FITC-anti-IgG.

was applied, the rings are nearly circular and the aspect ratio is about 1 (Figure 3d). After a force of 0.1, 0.3, and 0.6 N was applied, the rings changed from circular to elliptical with the aspect ratio of 1.5 (Figure 3e), 2 (Figure 3f), and 2.5 (Figure 3g). Besides, we can see that the order of the structures did not change after the stretch of the PDMS micromolds. These results indicate that the elliptical ring arrays with a larger aspect ratio can be fabricated via reasonable design and operation; meanwhile, the size of the polymer brush rings can be easily modulated via changing the diameter of the microspheres which were used as the original templates during the process of ring arrays fabrication by colloidal lithography dewetting. Figure S6 shows the images of the elliptical ring arrays which were fabricated by using the microspheres of different diameters as the original templates, and these results proved the maneuverability of this method in fabricating elliptical ring arrays.

3.3. Preparation of the Elliptical Protein Ring Arrays. Elliptical protein ring arrays are prepared via covalently immobilizing proteins on the PHEMA brush patterns. For the purposes of reducing the nonspecific absorption of proteins on the samples, a monolayer of PEG-silane is grafted onto the regions without ATRP initiator patterns before the polymerization of the PHEMA. After obtaining the elliptical PHEMA brush ring arrays via grafting the PHEMA from the surface of the ATRP initiator modified substrate as-prepared, the samples are immersed in a solution of 0.1 M DSC and DMAP in anhydrous DMF to obtain the succinimidyl group decorated PHEMA brush ring arrays. Then the protein ring arrays can be easily prepared by immersing the succinimidyl modified PHEMA ring arrays in the solution of human immunoglobulin G (IgG), since the succinimidyl group is highly reactive with the primary amine groups of the proteins. To confirm the human IgG is covalently grafted to the polymer brush and to evaluate the biological activity of IgG, negative control experiments were performed as mentioned and investigated by fluorescence microscopy under blue light excitation. Figure S1 shows the fluorescent photographs achieved from the negative control experiments. Figure S1a is the human IgG pattern prepared on the PHEMA ring arrays without the succinimidyl modification after binding FITC-labeled goat anti-human IgG. Figure S1b–d shows the human IgG patterns prepared on the activated PHEMA ring arrays after binding FITC-labeled BSA (Figure S1b), FITC-labeled rabbit anti-mouse IgG (Figure S1c), and FITC-labeled goat anti-human IgG (Figure S1d). Figure S1e–h shows the fluorescent photographs of the (a)–(d) samples after treatment with ultrasonication for 30 s and washing with the buffer solution respectively. From the comparison of Figure S1a, d, e, and h, we can see that, without the succinimidyl modification, human IgG just adheres to the surface via physical absorption rather than grafts to the polymer brush covalently with no ordered ring protein pattern achieved. However, for the succinimidyl modified one, the protein ring arrays were achieved via grafting the protein to the polymer brush covalently, which were stable enough for the pattern and could maintain their morphology after the ultrasonic treatment. These results indicated that the human IgG was grafted to the polymer brush through covalent reaction instead of physical absorption, which insures the stability of the protein patterns. Through the comparison of Figure S1b–d, f–h, the human IgG on the nanoring arrays maintains its biological activity, for the FITC-labeled goat anti-human IgG can react with human IgG specifically followed by the formation of visible protein patterns and the patterns are maintained after ultrasonic treatment. On the other hand, since FITC-labeled BSA and FITC-labeled goat anti-human IgG did not have the specificity to react with human IgG, there are no visible ordered protein patterns achieved and the FITC-labeled proteins were easily removed from the IgG patterns via ultrasonic treatment. These results proved that the FITC-labeled goat anti-human IgG combined with the human IgG on the polymer ring arrays via the specific interaction between antigen and antibody, and the human IgG maintain their biological activity. All of these data proved that proteins which have the amino group ($-NH_2$) can covalently graft to the polymer brush to form protein patterns and maintain biological activity by using this DSC active method. Figure 4 shows the fluorescence photographs of the IgG ring arrays with aspect ratio 1 (Figure 4a), 1.5 (Figure 4b), and 2.5 (Figure 4c). From the fluorescence photographs, we can see that the protein ring arrays are homogeneous over large areas and the signal intensity is nearly the same throughout the entire area, which proves that the protein ring arrays are finely prepared and the biological activity is maintained. Moreover, this kind of complex protein patterns can be used as new substrates to study the reactions of cell–substrate and cell–cell, since the protein patterns are held robustly in situ by covalent bonds. In addition, the polymer brushes act as linkers between the protein and substrate which is long enough to prevent the denaturation of proteins when they are absorbed onto the substrate.

3.4. Cell Adhesion on the Ring and Elliptical Ring Arrays. As we know, since the properties of the substrates and the interfaces between cell and substrate have great influence on cell adhesion and other behaviors, we need to fabricate different surfaces to make it clear how the surface or interfaces affect the cell behavior. Under this background, the ring arrays and elliptical ring arrays of protein are an ideal matrix which provides nice surfaces and interfaces to study the different

adhesion behaviors on holomorphic symmetry and unholomorphic symmetry substrates. The fibronectin (FN) ring arrays of the circular one and the elliptic one with the aspect ratio 2.5 were used to perform the experiment of cell culture. After culturing for 12 h, the actin cytoskeleton, cell nucleus, and vinculin were stained with TRITC-phalloidin, DAPI, and mouse monoclonal anti-vinculin/FITC-conjugated goat anti-mouse IgG, respectively. Figure 5 shows the confocal

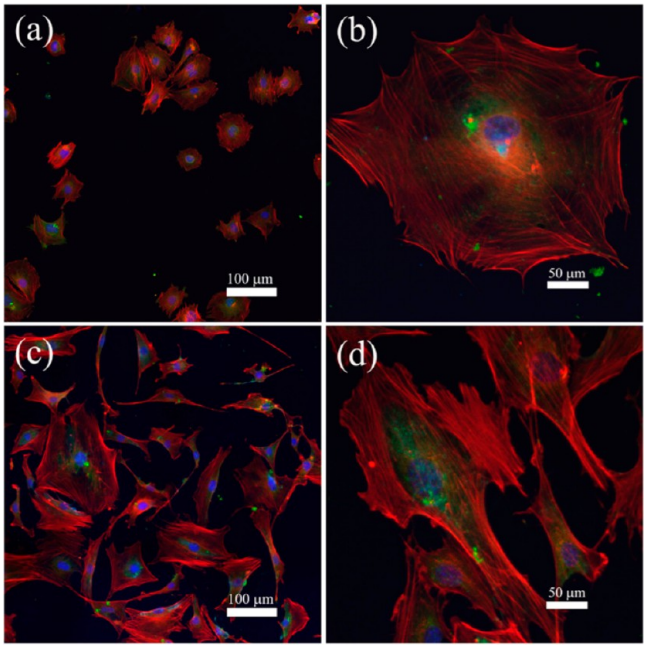

Figure 5. Confocal fluorescent microscopy images of the cell cultured on the ring (a,b) and elliptical ring (c,d) patterns: blue, nucleus; red, actin cytoskeleton; green, vinculin.

fluorescent microscopy images of the cell cultured on the ring (Figure 5a,b) and elliptical ring (Figure 5c,d) patterns with the stain colors of blue, red, and green representing the nucleus, the actin cytoskeleton, and vinculin, respectively. The images confirmed that mouse MC3T3-E1 osteblasts adhered well onto the FN modified substrates, for the FN can promote cell adhesion and the cells maintained good biological activity since the cells performed great degree of spreading on both substrates. However, the adhesion behaviors are different on the substrates with different physical features. The cells adhered to the FN ring arrays had disclike morphology with disordered spreads (Figure 5a), while the actin cytoskeleton showed a flexible state and assembled into a clewlike morphology (Figure 5b). However, the cells adhered to the elliptic one showed elongation profiles with much ordered spreads (Figure 5c), while the actin cytoskeleton showed a rigid state and mostly distributed on either side of the cell nuclei with a polarized orientation (Figure 5d). These results might be caused by the FN interface between cell and the substrate. For the ring one, the orientation of the isotropic microstructure could not provide the polarized induction, and the cells showed to be spread disordered since the environment around them is the same. However, for the elliptical one, the ratio of protein region at the long axis direction reached 78% while this value was just about 52% at the short axis direction; thus, the protein region provide more adhesion sites at the long axis direction than the short one which induced the cell spreading along the long axis direction. For the same reason, the elliptical protein ring provides more adhesion sites along the long axis direction. There might be more feet to anchor to the protein pattern than the short one, so it may efficiently promote the orientation of the skeleton along the long axis and be rigid. For the cells on the ring pattern, each direction provides the equal chance to anchor, so the stretch force from different directions is the same which made the skeleton be clewlike and seem flexible. These phenomena show that the surface or interface which contains protein patterns had an active influence on cell adhesion behaviors which might be useful in tissue engineering in the future. In addition, the cell behaviors on this 3D substrate are different from that of the cells adhered to the 2D patches as reported by another group.[54,55] In our experiment, the spread area of the cytoskeleton is larger than the focal adhesion which is different in that the focal adhesion area is much larger than the cytoskeleton. Besides, there is no fusiform focal adhesion formed at the periphery of the cell which is obviously seen on the 2D patch surfaces (Figure S2). These results proved that the symmetry of underlying structure had a great effect on cell adhesion behaviors and the formation of the actin cytoskeleton. Further experiments need to be done to allow us to draw more specific conclusions.

4. CONCLUSION

In summary, a novel method to fabricate elliptical protein ring arrays with controllable feature parameters which were mediated by elliptical polymer brush ring arrays is presented. By this method, elliptical protein ring arrays with different aspect ratios and feature sizes can be prepared over a large area. Moreover, the as-prepared arrays of FN can be used to study the cell adhesion behaviors and the morphogenesis of the actin cytoskeleton. As a result, the protein arrays are very promising surfaces for cell−substrate interactions, cell−cell interactions, and extensive investigations in biomaterials and related areas. Due to the high-throughput, parallel fabrication, and cost-efficiency, this method is readily accessible to researchers in many fields, including microfluidics, biosensors, and fundamental biology studies. Moreover, the elliptical polymer brush nanoring arrays have potential applications in fabrication of metal nanoring arrays, oil−water separation, and multiple detection.

■ ASSOCIATED CONTENT

Supporting Information

Additional figures as described in the text. This material is available free of charge via the Internet at http://pubs.acs.org

■ AUTHOR INFORMATION

Corresponding Author

*E-mail: byangchem@jlu.edu.cn. Fax: +86 431 85193423. Tel: +86 431 85168478.

Notes

The authors declare no competing financial interest.

■ ACKNOWLEDGMENTS

This work was supported by the National Science Foundation of China (Grand No.91123031, 21221063) and the National Basic Research Program of China (973 project, 2012CB933800).

REFERENCES

(1) Xu, L.; Vemula, S. C.; Jain, M.; Nam, S. K.; Donnelly, V. M.; Economou, D. J.; Ruchhoeft, P. *Nano Lett.* **2005**, *5*, 2563−2568.
(2) Pan, Z.; Alem, N.; Sun, T.; Dravid, V. P. *Nano Lett.* **2006**, *6*, 2344−2348.
(3) Kumar, A.; Biebuyck, H. A.; Whitesides, G. M. *Langmuir* **1994**, *10*, 1498−1511.
(4) Lian, J.; Wang, L.; Sun, X.; Yu, Q.; Ewing, R. C. *Nano Lett.* **2006**, *6*, 1047−1052.
(5) Singh, G.; Griesser, H. J.; Bremmell, K.; Kingshott, P. *Adv. Funct. Mater.* **2011**, *21*, 540−546.
(6) Valsesia, A.; Colpo, P.; Mannelli, I.; Mornet, S.; Bretagnol, F.; Ceccone, G.; Rossi, F. *Anal. Chem.* **2008**, *80*, 1418−1424.
(7) Lee, K.-B.; Kim, E.-Y.; Mirkin, C. A.; Wolinsky, S. M. *Nano Lett.* **2004**, *4*, 1869−1872.
(8) Coyer, S. R.; Delamarche, E.; García, A. J. *Adv. Mater.* **2011**, *23*, 1550−1553.
(9) Gaster, R. S.; Hall, D. A.; Wang, S. X. *Nano Lett.* **2010**, *11*, 2579−2583.
(10) Alang Ahmad, S. A.; Wong, L. S.; ul-Haq, E.; Hobbs, J.; Leggett, G. J.; Micklefield, J. *J. Am. Chem. Soc.* **2011**, *133*, 2749−2759.
(11) Curtis, A.; Riehle, M. *Phys. Med. Biol.* **2001**, *46*, R47−65.
(12) Kam, L.; Shain, W.; Turner, J. N.; Bizios, R. *Biomaterials* **1999**, *20*, 2343−2350.
(13) Gurkan, U. A.; Fan, Y.; Xu, F.; Erkmen, B.; Urkac, E. S.; Parlakgul, G.; Bernstein, J.; Xing, W.; Boyden, E. S.; Demirci, U. *Adv. Mater.* **2013**, *25*, 1192−1198.
(14) Park, J. W.; Kim, H. J.; Kang, M. W.; Jeon, N. L. *Lab Chip* **2013**, *13*, 509−521.
(15) Christman, K. L.; Enriquez-Rios, V. D.; Maynard, H. D. *Soft Matter* **2006**, *2*, 928−939.
(16) Jonkheijm, P.; Weinrich, D.; Schroder, H.; Niemeyer, C. M.; Waldmann, H. *Angew. Chem., Int. Ed.* **2008**, *47*, 9618−9647.
(17) Torres, A. J.; Wu, M.; Holowka, D.; Baird, B. *Annu. Rev. Biophys.* **2008**, *37*, 265−288.
(18) Bettinger, C. J.; Langer, R.; Borenstein, J. T. *Angew. Chem., Int. Ed.* **2009**, *48*, 5406−5415.
(19) Kim, D.-H.; Lee, H.; Lee, Y. K.; Nam, J.-M.; Levchenko, A. *Adv. Mater.* **2010**, *22*, 4551−4566.
(20) Taylor, Z. R.; Patel, K.; Spain, T. G.; Keay, J. C.; Jernigen, J. D.; Sanchez, E. S.; Grady, B. P.; Johnson, M. B.; Schmidtke, D. W. *Langmuir* **2009**, *25*, 10932−10938.
(21) Schlapak, R.; Danzberger, J.; Haselgrubler, T.; Hinterdorfer, P.; Schaffler, F.; Howorka, S. *Nano Lett.* **2012**, *12*, 1983−1989.
(22) Zhao, B.; Brittain, W. J. *Prog. Polym. Sci.* **2000**, *25*, 677−710.
(23) Barbey, R.; Lavanant, L.; Paripovic, D.; Schuwer, N.; Sugnaux, C.; Tugulu, S.; Klok, H. A. *Chem. Rev.* **2009**, *109*, 5437−5527.
(24) Ducker, R.; Garcia, A.; Zhang, J.; Chen, T.; Zauscher, S. *Soft Matter* **2008**, *4*, 1774−1786.
(25) Tugulu, S.; Harms, M.; Fricke, M.; Volkmer, D.; Klok, H.-A. *Angew. Chem. Int. Ed.* **2006**, *45*, 7458−7461.
(26) Jeon, H.; Schmidt, R.; Barton, J. E.; Hwang, D. J.; Gamble, L. J.; Castner, D. G.; Grigoropoulos, C. P.; Healy, K. E. *J. Am. Chem. Soc.* **2011**, *133*, 6138−6141.
(27) Zhou, F.; Jiang, L.; Liu, W.; Xue, Q. *Macromol. Rapid Commun.* **2004**, *25*, 1979−1983.
(28) Ahn, S. J.; Kaholek, M.; Lee, W. K.; LaMattina, B.; LaBean, T. H.; Zauscher, S. *Adv. Mater.* **2004**, *16*, 2141−2145.
(29) Paik, M. Y.; Xu, Y.; Rastogi, A.; Tanaka, M.; Yi, Y.; Ober, C. K. *Nano Lett.* **2010**, *10*, 3873−3879.
(30) He, Q.; Kueller, A.; Schilp, S.; Leisten, F.; Kolb, H.-A.; Grunze, M.; Li, J. *Small* **2007**, *3*, 1860−1865.
(31) Schmelmer, U.; Paul, A.; Kuller, A.; Steenackers, M.; Ulman, A.; Grunze, M.; Golzhauser, A.; Jordan, R. *Small* **2007**, *3*, 459−465.
(32) Liu, X.; Guo, S.; Mirkin, C. A. *Angew. Chem., Int. Ed.* **2003**, *42*, 4785−4789.
(33) Zhou, X.; Wang, X.; Shen, Y.; Xie, Z.; Zheng, Z. *Angew. Chem., Int. Ed.* **2011**, *50*, 6506−6510.
(34) Zhou, F.; Zheng, Z.; Yu, B.; Liu, W.; Huck, W. T. *J. Am. Chem. Soc.* **2006**, *128*, 16253−16258.
(35) Chen, T.; Jordan, R.; Zauscher, S. *Small* **2011**, *7*, 2148−2152.
(36) Pernites, R. B.; Foster, E. L.; Felipe, M. J.; Robinson, M.; Advincula, R. C. *Adv. Mater.* **2011**, *23*, 1287−1292.
(37) Khanduyeva, N.; Senkovskyy, V.; Beryozkina, T.; Horecha, M.; Stamm, M.; Uhrich, C.; Riede, M.; Leo, K.; Kiriy, A. *J. Am. Chem. Soc.* **2008**, *131*, 153−161.
(38) Brinks, M. K.; Hirtz, M.; Chi, L.; Fuchs, H.; Studer, A. *Angew. Chem., Int. Ed.* **2007**, *46*, 5231−5233.
(39) Benetti, E. M.; Acikgoz, C.; Sui, X.; Vratzov, B.; Hempenius, M. A.; Huskens, J.; Vancso, G. J. *Adv. Funct. Mater.* **2011**, *21*, 2088−2095.
(40) Lee, B. K.; Lee, H. Y.; Kim, P.; Suh, K. Y.; Seo, J. H.; Cha, H. J.; Kawai, T. *Small* **2008**, *4*, 342−348.
(41) Hoff, J. D.; Cheng, L.-J.; Meyhöfer, E.; Guo, L. J.; Hunt, A. J. *Nano Lett.* **2004**, *4*, 853−857.
(42) Maury, P.; Escalante, M.; Péter, M.; Reinhoudt, D. N.; Subramaniam, V.; Huskens, J. *Small* **2007**, *3*, 1584−1592.
(43) Coyer, S. R.; Garcia, A. J.; Delamarche, E. *Angew. Chem., Int. Ed.* **2007**, *46*, 6837−6840.
(44) Zheng, Y. B.; Wang, S. J.; Huan, A. C. H.; Wang, Y. H. *J. Non-Cryst. Solids* **2006**, *352*, 2532−2535.
(45) Wen, Z. C.; Wei, H. X.; Han, X. F. *Appl. Phys. Lett.* **2007**, *91*, 122511−122513.
(46) Larsson, E. M.; Alegret, J.; Käll, M.; Sutherland, D. S. *Nano Lett.* **2007**, *7*, 1256−1263.
(47) Choi, H. W.; Jeon, C. W.; Liu, C.; Watson, I. M.; Dawson, M. D.; Edwards, P. R.; Martin, R. W.; Tripathy, S.; Chua, S. J. *Appl. Phys. Lett.* **2005**, *86*, 021101−021103.
(48) Bary-Soroker, H.; Entin-Wohlman, O.; Imry, Y. *Phys. Rev. B* **2010**, *82*, 144202.
(49) Bleszynski-Jayich, A. C.; Shanks, W. E.; Peaudecerf, B.; Ginossar, E.; von Oppen, F.; Glazman, L.; Harris, J. G. *Science* **2009**, *326*, 272−275.
(50) Zhu, J.-G.; Youfeng, Z.; Prinz, G. A. *J. Appl. Phys.* **2000**, *87*, 6668−6673.
(51) Aizpurua, J.; Hanarp, P.; Sutherland, D. S.; Kall, M.; Bryant, G. W.; Garcia de Abajo, F. J. *Phys. Rev. Lett.* **2003**, *90*, 057401.
(52) Winzer, M.; Kleiber, M.; Dix, N.; Wiesendanger, R. *Appl. Phys. A* **1996**, *63*, 617−619.
(53) Li, Y.; Zhang, J.; Fang, L.; Jiang, L.; Liu, W.; Wang, T.; Cui, L.; Sun, H.; Yang, B. *J. Mater. Chem.* **2012**, *22*, 25116−25122.
(54) Malmström, J.; Lovmand, J.; Kristensen, S.; Sundh, M.; Duch, M.; Sutherland, D. S. *Nano Lett.* **2011**, *11* (6), 2264−2271.
(55) Malmström, J.; Christensen, B.; Jakobsen, H. P.; Lovmand, J.; Foldbjerg, R.; Sørensen, E. S.; Duncan, S.; Sutherland, D. S. *Nano Lett.* **2010**, *10*, 686−694.
(56) Dong, R.; Krishnan, S.; Baird, B. A.; Lindau, M.; Ober, C. K. *Biomacromolecules* **2007**, *8*, 3082−3092.
(57) Barbey, R.; Kauffmann, E.; Ehrat, M.; Klok, H.-A. *Biomacromolecules* **2010**, *11*, 3467−3479.